Pores in fractal aerogels and their incidence on scaling

1991 J. Phys.: Condens. Matter 3 6531

(http://iopscience.iop.org/0953-8984/3/33/027)

J. Phys.: Condens. Matter 3 (1991) 6531–6545. Printed in the UK

COMMENT

Pores in fractal aerogels and their incidence on scaling

R Vacher†, E Courtens‡, E Stoll‡, M Böffgen§ and H Rothuizen‡

† Laboratoire de Science des Matériaux Vitreux, Université de Montpellier II, F-34095, Montpellier, France

‡ IBM Research Division, Zurich Research Laboratory, CH-8803 Rüschlikon, Switzerland

§ Villeroy & Boch AG, Forschungszentrum-Zentrallabor, D-W 6642 Mettlach, Federal Republic of Germany

Received 25 March 1991, in final form 8 May 1991

Abstract. The nature of scanning electron-microscopy images of silica aerogels is shown to depend enormously on the conductive coating used. The analysis of such images, and of a large amount of other data, confirms that our samples become homogeneous at the point where their fractal regime terminates. There is no disturbing macroporosity that would prevent scaling in function of the density. Simulations of a very large percolation model confirm that the scaling law is obeyed by the pore-size distribution and emphasize that a few occurrences of large pores are to be expected in disordered fractals. The results also clarify the distinction between the acoustic and density correlation lengths.

1. Introduction

Currently there is great interest in fractal materials (Fleischmann *et al* 1989), and particularly in silica aerogels which appear to be excellent realizations of fractal solids. Structural studies (Schmidt 1991) as well as experiments on the dynamics involved (Richter *et al* 1989) have been recently reviewed. The availability of aerogels has allowed the theory of fractons (Alexander and Orbach 1982) to be tested for the first time on samples whose fractal structure could be unambiguously demonstrated and characterized. In particular, the ability to prepare 'mutually self-similar' sample series was revealed by small angle neutron scattering (SANS) measurements (Vacher *et al* 1988). The availability of such series allowed the fractal dimension D and the fracton dimension $\tilde{d}$ to be extracted from the scaling of Brillouin-scattering data (Courtens *et al* 1987, 1988). The result for D agreed with the previous structural determination, whereas that for $\tilde{d}$ has now been confirmed by extensive neutron-scattering measurements of the density of vibrational states (Courtens *et al* 1990, Vacher *et al* 1990a). Raman scattering on aerogels also revealed the existence of fractons over the entire frequency range (Tsujimi *et al* 1988), with the scaling of the scattered intensity depending on an additional internal length index, σ, introduced by Alexander (1989).

In a recent publication, Rousset *et al* (1990) presented electron-microscopy images which they used to re-examine some of the above results. Their analysis led them to conclusions in contradiction with our previous interpretations. Thus we considered it important to reproduce carefully scanning electron-microscopy (SEM) measurements on the same materials. These are aerogels belonging to the mutually self-similar series of

0953-8984/91/336531 + 15 $03.50

so-called 'neutrally reacted' samples (Vacher *et al* 1988) on which most results quoted above were obtained. Our new SEM images are presented in the following section, where it is shown that sample preparation plays an enormous role in their nature. The correct interpretation of the observed pore sizes also requires a better understanding of the meaning of the fractal persistence length ξ in real space. This can be gained by the simulations presented in section 3. Thus equipped, we can re-examine the quantitative estimates presented by Rousset *et al* and find that our previous interpretations are vindicated.

2. Scanning electron-microscopy images

SEM and transmission electron-microscopy (TEM) have already been used extensively to investigate the structure of aerogels (Fricke 1986, Bourret 1988, Vacher *et al* 1989). The experiments revealed tenuous structures assembled from small particles. For many reasons, a strict quantitative interpretation of images of low-density microcellular materials should be treated with caution, as recently discussed by LeMay *et al* (1990). Of the many possible pitfalls in SEM, one might mention the difficulty of extracting average morphologies from local observations, the problem of obtaining 3D information from 2D projections, and especially the fact that the observed surface is always a fracture, which might not be typical of the bulk. Furthermore, for insulating samples, the surface must generally be coated with a conducting layer. This process is far from trivial for a tenuous material, and it can have dramatic effects on fragile structures as we are about to demonstrate. An alternative approach is to use uncoated samples. However, this affects the resolution owing to charging effects (Bourret 1988).

In spite of these considerations, the fact that the images of the materials obtained by Rousset *et al* (1990) had a peculiar grainy appearance prompted us to reproduce them. These images had been obtained with a gold coating. Gold is well known, particularly among biologists, to limit the resolution of SEM pictures significantly, as it tends to clump. This indicates a large surface tension that could even break aerogels in their weakest regions. On the other hand, Pt/C coatings are known to give generally excellent results for fragile samples. We show in figure 1 images obtained with the same three aerogels used by Rousset *et al* (1990) with the two different coatings. The pictures were taken with secondary electrons, using a Hitachi S4000 SEM. The samples belong to the series of materials, presented in figure 1, of Vacher *et al* (1988). They have been oxidized, as described in that reference, fractured in air, and evacuated for a long period at a slightly elevated temperature before the application of the coatings, which are typically of the order of 10 to 20 nm thick.

The differences between the left and right sides of figure 1 are remarkable. On the left, one recognizes the 'grains' reported by Rousset *et al*, the mean size of which tends to increase as the density of the aerogel decreases. The grains show a microstructure at a scale of the order of 10 nm, typical for gold crystallization. The grains are well separated, giving the visual impression of a large inter-grain porosity (the dark areas between the grains). On the right of figure 1, by contrast, one notes that the structure becomes finer as the density is decreased. Clearly the Pt/C coating preserves part of the fractal structure of the lightest sample. It does not have the mobility of gold, and thus forms neither the fine microstructure nor the large clumps that appear on the left-hand side. The latter might result from local damages produced by capillary forces. On the Pt/C images, some fairly large holes can be seen on the fractured surfaces, and a few of

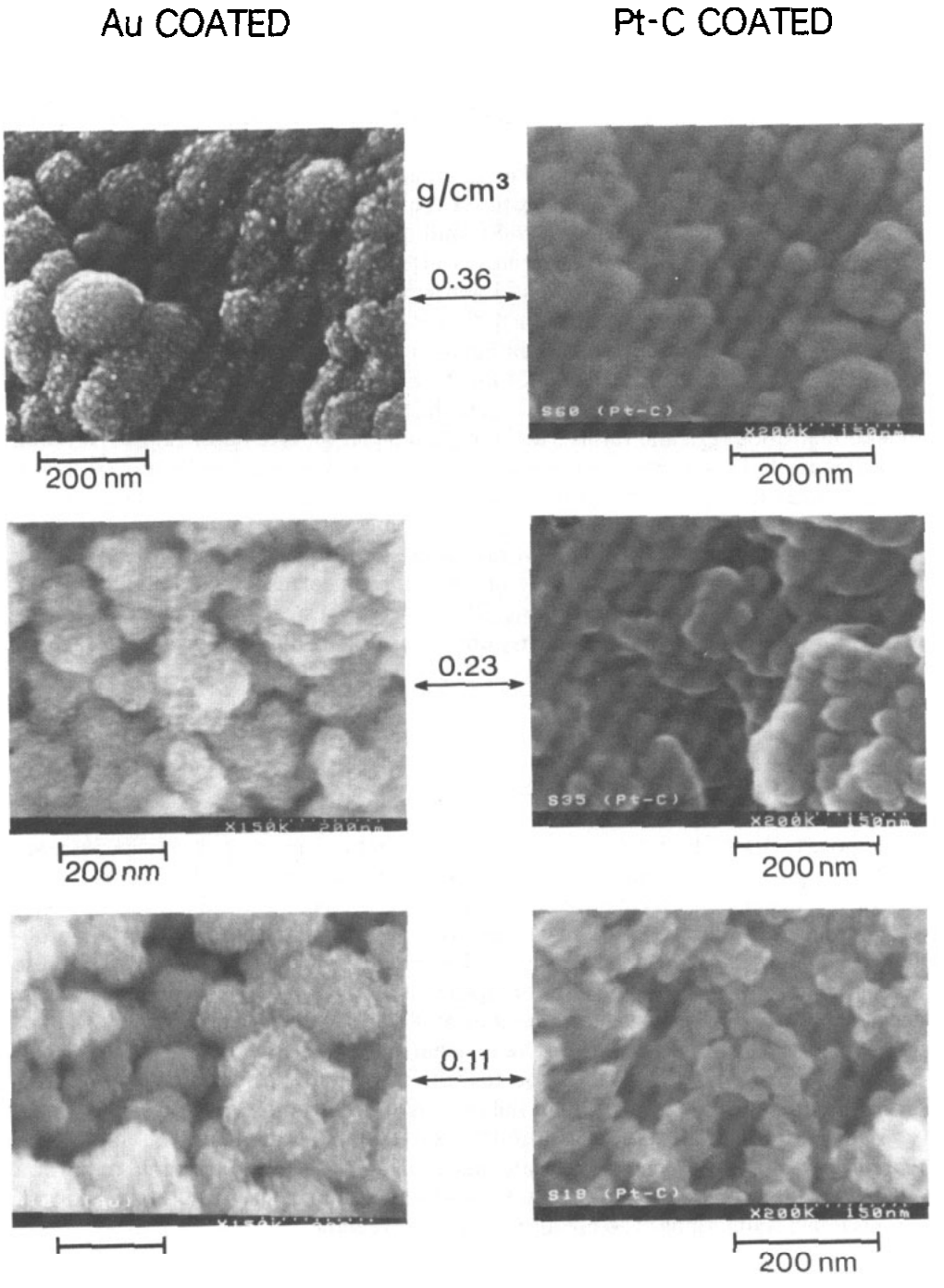

Figure 1. Scanning electron-microscopy pictures obtained on the three samples $\rho = 0.36$ g cm^{-3} on top, $\rho = 0.23$ g cm^{-3} in the middle, and $\rho = 0.11$ g cm^{-3} at the bottom. The left side shows surfaces with a gold coating, while the right side shows them with the Pt/C coating. The lighter areas must be understood as being above the darker ones. The very dark ones are 'pores'.

these might be real pores, corresponding to the dark areas going deep into the material. However, one does not gain the impression that the materials are 'large scale aggregates of grains' as is the case for images with gold. As discussed in the next section, the occurrence of a few pores whose size can be significantly larger than the fractal persistence length ξ is intrinsic to disordered fractal structures, and consistent with the images on the right-hand side.

It is thus of interest to present, in more detail, the images obtained with the Pt/C coated samples: figures 2–4. We indicate in these figures two distinct values of ξ: ξ_ρ measured with SANS (Vacher *et al* 1988), and ξ_{ac} derived from the phonon–fracton crossover observed in Brillouin scattering (Courtens *et al* 1988). The measured ratio ξ_{ac}/ξ_ρ is between 4 and 5 for this series of aerogels (Courtens and Vacher 1989). This observation will be explained in section 4. Considering figures 2 to 4, one first notes that at the largest scale the materials look rather homogeneous, with no indications of large macropores. The fractures are rougher for the lighter samples, as expected. The high resolution pictures reveal an appreciable number of pores starting at a scale equal to or smaller than about ξ_{ac}, and this is true for each sample. Surface depressions associated with fracture steps, particularly obvious at the intermediate density (figure 3), should not be confused with the real pores which are the very dark areas. Interestingly, the values of ξ_{ac} correspond to the size of the 'grains' measured by Rousset *et al* (1990), as listed in table 1. Finally, one notes that no fractal structure can be recognized in any of these images below a scale of about 20 nm, which must correspond to the filling of the inter-particle space by the Pt/C coating. Thus, no fractal structure can be seen for the density $\rho = 0.36\ \mathrm{g\ cm^{-3}}$, whereas nearly one order of magnitude of the fractal range is seen for $\rho = 0.11\ \mathrm{g\ cm^{-3}}$.

3. Simulations of pore-size distribution

On regular fractals which have been constructed up to a maximum fractal persistence length ξ (e.g. a Sierpinski gasket or a Menger sponge), there exists a pore of maximum size of the order of ξ. By contrast, for disordered fractals (e.g. for a large infinite percolation cluster above the percolation threshold p_c) there is always a certain probability of finding pores much larger than ξ. These rare occurrences do not prevent these models from being macroscopically homogeneous above ξ in the sense that the average density about an occupied site becomes independent of scale at scales sufficiently larger than ξ. In discussing 'macropores' in a real fractal material, it is important to understand how many large pores are to be expected due to fractality as opposed to an excess probability that would make the material macroscopically inhomogeneous.

To develop a feeling for this, it is useful to resort to simulations. It must be emphasized that our present purpose is not to create images of aerogels to be compared to the SEM ones. It is rather to understand the 'bulk' distribution of pore sizes in a random fractal. To this effect simulations in 2D are already quite revealing.

3.1. Structure of a large percolation cluster above threshold

Figure 5 presents the percolating cluster on a 6800^2 site-percolation network at the occupation probability $p = p_c + 0.00845$. The relatively high value of $p - p_c$ was selected in order to achieve a sufficiently short fractal persistence length ξ, which allows us to

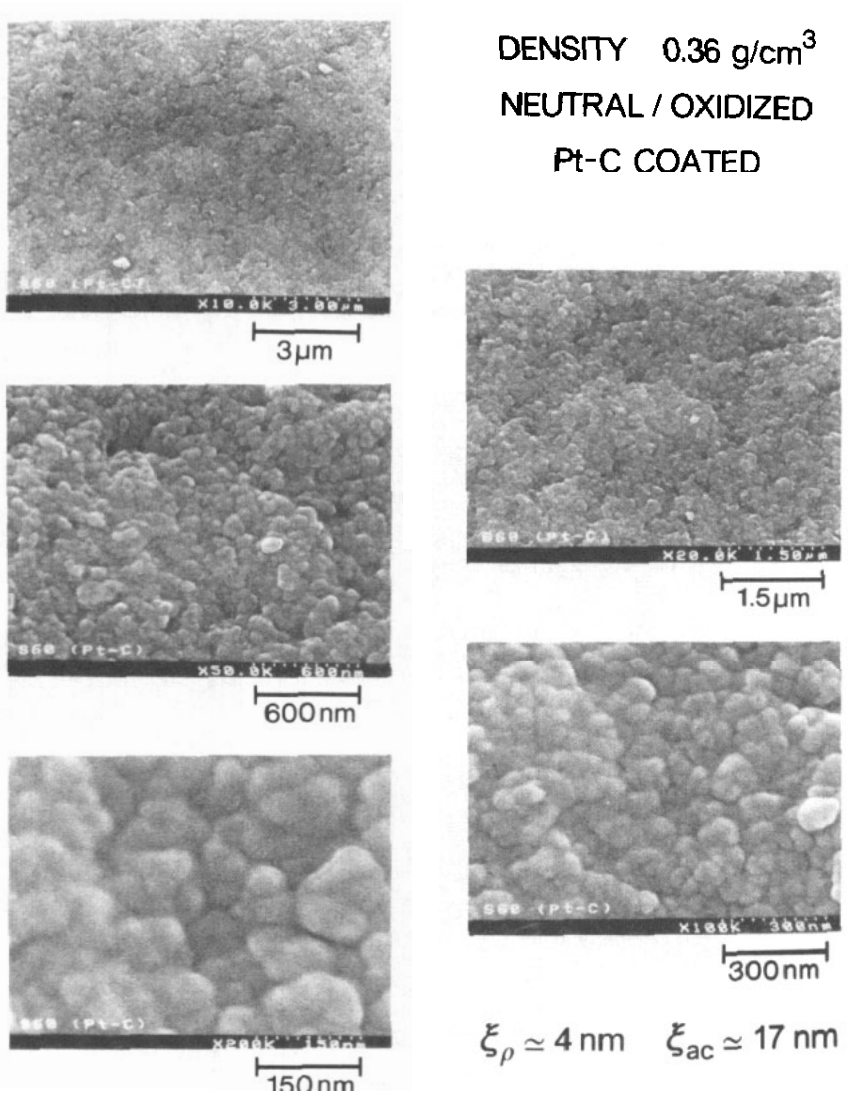

Figure 2. SEM pictures of the Pt/C coated $\rho = 0.36\,\mathrm{g\,cm^{-3}}$ sample under different magnifications. The successive pictures are magnifications of the centre of the previous ones. This allows one mentally to zoom-in on the sample, to follow the evolution of the various features as a function of the magnification.

observe what happens at scales much beyond ξ where the cluster becomes homogeneous. Additional pictures of that cluster have been presented elsewhere (Vacher *et al* 1990b). The cluster is sufficiently large for excellent statistics of all quantities of interest in the fractal region to be obtained from this single realization. The persistence length ξ can be estimated from the pair correlation function $g(\boldsymbol{r})$,

$$g(\boldsymbol{r}) = \sum_{i \neq 0} \langle \delta(\boldsymbol{r} - \boldsymbol{R}_i + \boldsymbol{R}_0) \rangle. \tag{1}$$

In this expression the sum of δ-functions is taken over all occupied sites at positions

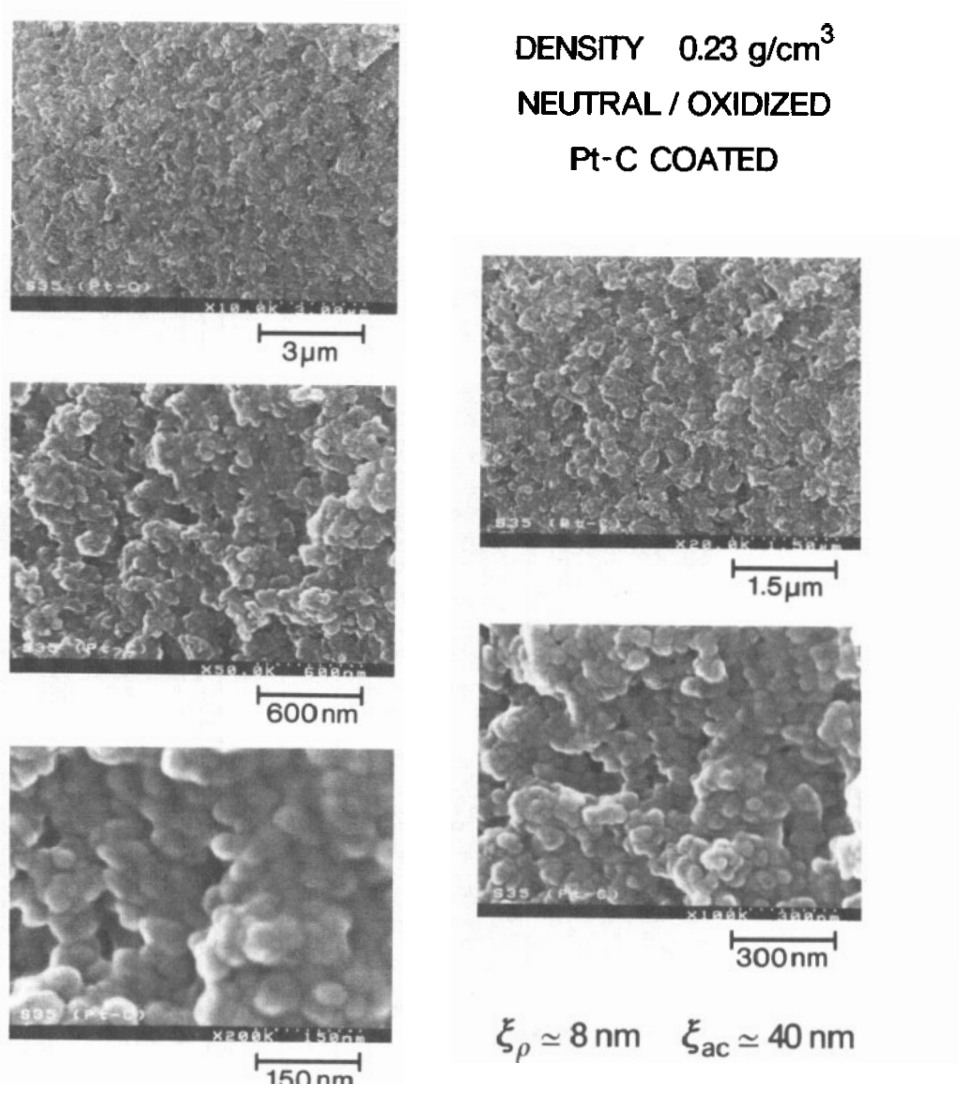

Figure 3. SEM pictures of the Pt/C coated $\rho = 0.23\,\mathrm{g\,cm^{-3}}$ sample under different magnifications, as in figure 2.

$\boldsymbol{R}_j$; $\boldsymbol{R}_0$ is the position vector of an occupied site selected as origin, and the angular brackets designate an average over these origins. In the fractal regime, the properly smoothed $g(\boldsymbol{r})$ scales as

$$g(r) \propto \rho(r) \propto (r/b)^{D-d} \tag{2}$$

where $\rho(\boldsymbol{r})$ is the average density in a circle of radius r centred on an occupied site (see, e.g. Kapitulnik *et al* 1983). Here, d is the Euclidean dimension, and b is the unit-cell size of the square network over which the percolation cluster is constructed. It is evident that $g(r) \propto \rho(r)$, since the latter is simply the surface integral of the former normalized

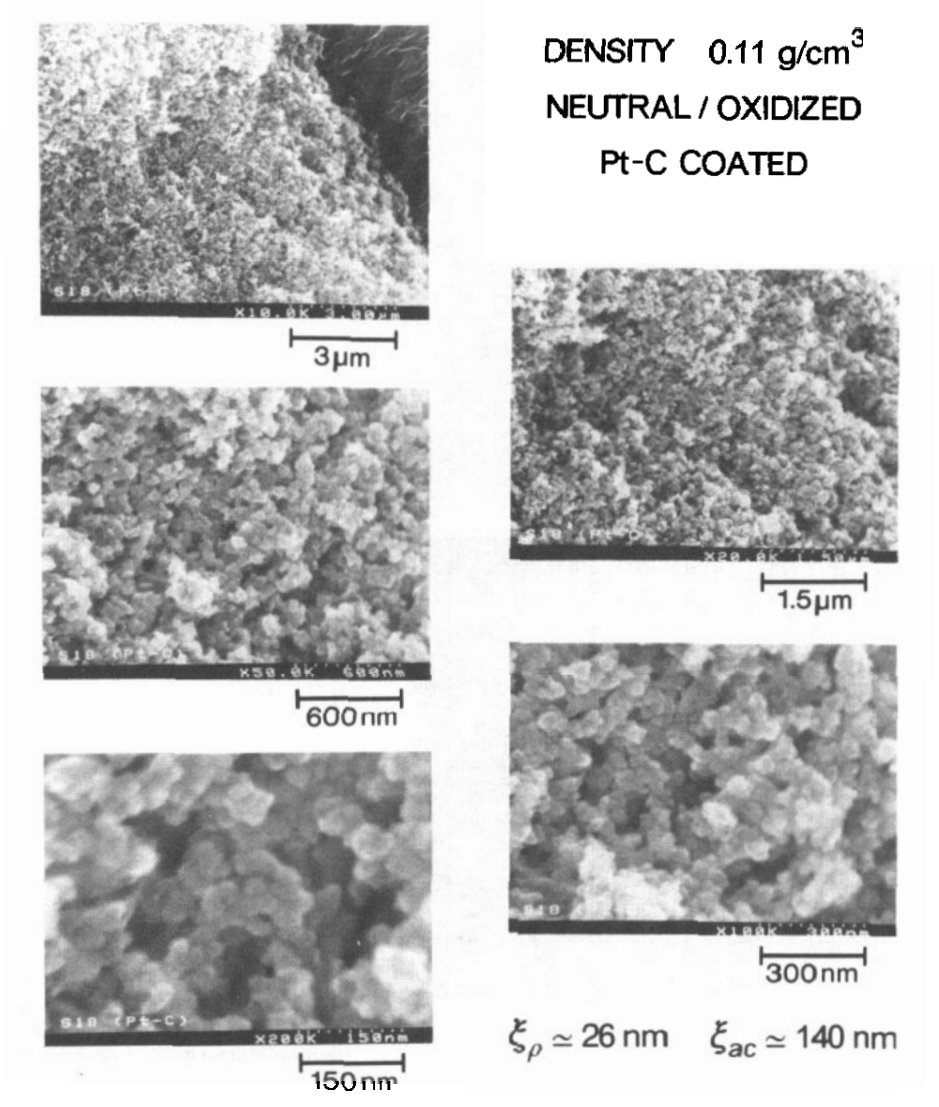

Figure 4. SEM pictures of the Pt/C coated $\rho = 0.11$ g cm^{-3} sample under different magnifications, as in figure 2.

Table 1. Parameters of the investigated samples.

Aerogel density ρ (g cm^{-3})	0.36	0.23	0.11
Density correlation length ξ_ρ (nm)	4	8	26
Acoustic correlation length ξ_{ac} (nm)	17	40	140*
Ornstein–Zernike diameter $2r_0 = 2\sqrt{5}\xi_\rho$ (nm)	18	36	116
'Grain' size from Rousset *et al* (1990) (nm)	13	27	50
Cluster density $\rho(r_0)$ (g cm^{-3})	0.48	0.32	0.16

* Extrapolated value from Courtens and Vacher (1989).

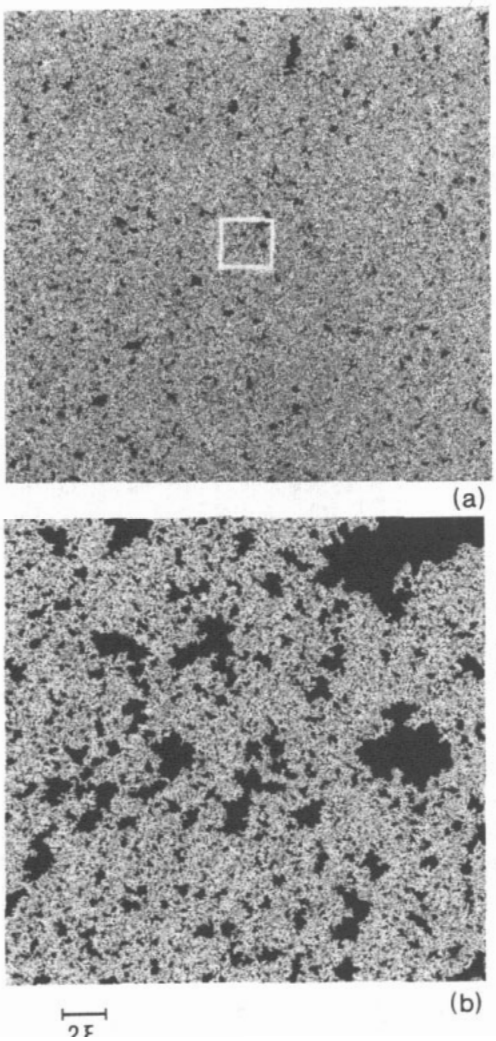

Figure 5. Simulation of the site percolation at $p - p_c = 0.00845$. Only the percolating cluster is shown (light areas): (*a*) is the full 6800^2 simulation whereas (*b*) shows the centre of (*a*) magnified 10 times; the size $2\xi_\rho$ is indicated. A few large pores are evident in (*a*), whereas the large number of pores of size up to $2\xi_\rho$ is easily seen in (*b*).

by the area of integration, so that both scale with the same exponent. Far into the homogeneous regime, $g(r)$ equals ρ, the macroscopic density of occupied sites.

Figure 6*a* shows the pair correlation calculated on the cluster of figure 5*a*, with r in the direction of the coordinate axes of the underlying square lattice. The length ξ can be derived from the position of the intercept of the asymptotic fractal and homogeneous regimes. The fractal range being small, the slope of the straight line in the fractal regime is taken from $D = 91/48$ (Stauffer 1986). The intercept of the two lines in figure 6*a* is at a value ξ_g which is different from the ξ_ρ that would be obtained from a similar plot of $\rho(r)$. Given the surface integration connecting $g(r)$ with $\rho(r)$, one derives $\xi_\rho = (2/D)^{1/(2-D)}\xi_g$. The intercept in figure 6*a* gives $\xi_g \simeq 16b$. The corresponding value of ξ_ρ is in good agreement with that derived from fitting the structure factor $S(q)$ at small q-values. This was done with the heuristic expression $S(q) \propto [1 + (q\xi_\rho)^2]^{-D/2}$ (Teixeira

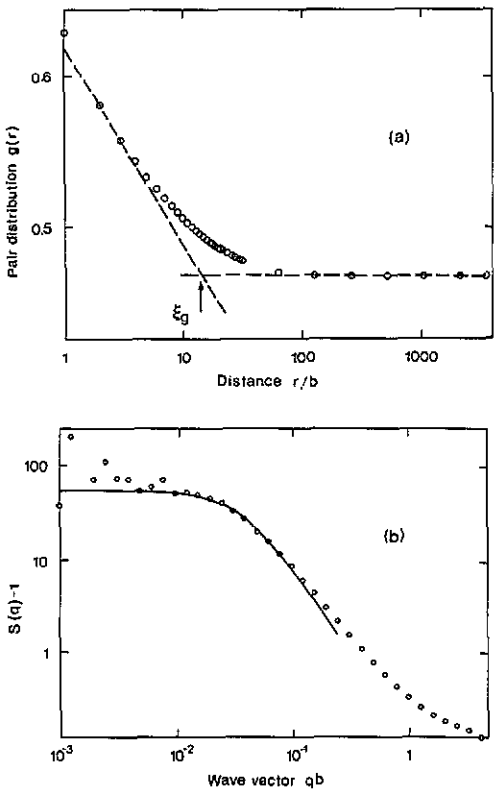

Figure 6. (*a*) The pair correlation function $g(r)$ for the cluster in figure 5*a* with the lines indicating the asymptotic regimes; (*b*) the structure factor $S(q)$ fitted to the heuristic Ornstein–Zernike-like expression.

1986) and it is shown in figure 6*b*. From both figures 6*a* and 6*b* one derives $\xi_\rho = (28 \pm 3)b$. This is the Ornstein–Zernike ξ associated with the density correlation function.

3.2. Pore-size distribution

Inspection of figure 5 reveals that a large number of pores exist with a linear dimension up to at least $2\xi_\rho$, and that there are a few very large pores having a linear size larger than $10\xi_\rho$. In two dimensions, a pore can be defined as an empty area completely disconnected from other empty areas; two empty sites touching only by their corners are disconnected. Such a clear-cut definition does not hold in three dimensions, where it is common practice to speak of pores of different 'sizes' for systems of voids that might in fact be completely connected in a strict sense. We return to the latter case in section 4.3. The pore-size distribution calculated for the cluster in figure 5*a* is illustrated in figure 7. Figure 7*a* shows the probability of a site belonging to a pore of area smaller than or equal to L^2, designated by $P(L)$. The quantity is proportional to the cumulated pore area. Its derivative, dP/dL, shown in figure 7*b*, is simply the probability that a site belongs to a pore of size L^2. Consider now a fractal cluster of size L^2 centred on an occupied site. The pores it contains have a maximum linear size of $\sim L$. The occupied surface area is $\sim L^2\rho(L)$, while the pore area is $\sim L^2[1 - \rho(L)]$. Hence,

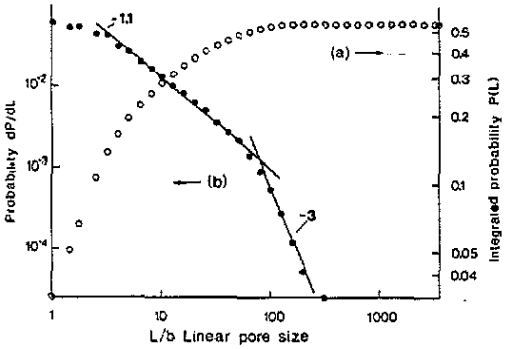

Figure 7. (a) The probability $P(L)$ of a site belonging to a pore of size less than or equal to L^2; (b) the derivative dP/dL with the fractal and homogeneous regimes shown by straight lines.

$P(L) \sim 1 - \rho(L)$, which has no straight part in the logarithmic presentation in figure 7*a*. However, the derivative

$$dP(L)/dL \propto -d\rho(L)/dL \propto (L/b)^{D-d-1} \tag{3}$$

has an extended region that is found to scale with the expected power -1.1, as shown in figure 7*b*. It is remarkable that this scaling extends to $L \approx 2\xi_\rho$, beyond which there is a sharp crossover to another regime, which for the available size of this simulation may be characterized by an effective exponent ≈ -3. From figure 7*a* we can see that the value of L is between ξ_ρ and $2\xi_\rho$ for 12.6% of the total pore area, and that L is greater than $2\xi_\rho$ in another 12.8% of the area. Some of these areas appear as 'macropores', the largest of which in this realization, near the upper edge of figure 5*a*, has an area of approximately 10^5 or about 100 times ξ_ρ^2. For an area enclosed by an isolated circle, the diameter equals four times the Ornstein–Zernike correlation length. This suggests that the largest fractal blobs in this simulation have a linear size of about $4\xi_\rho$. The packing of blobs of that approximate size happens to be consistent with voids of area of the order of $4\xi_\rho^2$. It is at the latter pore-size value that the crossover between fractal and homogeneous behaviour is observed in figure 7*b*. Semi-quantitative considerations of a similar nature will turn out to be relevant for estimates to be made in the next section.

4. Quantitative estimates

4.1. Size of the particles and their Raman scattering

The most reliable average information on the structure of these materials is obtained by small-angle-scattering determination of the structure factor, $S(q)$. At large q-values, the crossover between the bulk fractal and surface Porod regimes depends on the particle size. Although the Porod region is not very extensive in the materials investigated presently, the crossover is very clear, particularly in oxidized samples, as shown in figure 3 of Vacher *et al* (1988). The position of the crossover is at $q_{co} \approx 0.15$ Å^{-1}. For particles of volume V and surface S, the position of the crossover, defined as the intercept of the q^0 and q^{-4} asymptotic regimes in a logarithmic plot, is given by

$$q_{co} = (2\pi S/V^2)^{1/4} \tag{4}$$

as derived by Porod (1951). For spheres of diameter $2a$, this gives

$$a = (9/2)^{1/4}/q_{co}. \tag{5}$$

For shapes not too unlike spheres, including ellipsoids and cylinders with an elongation

ratio up to 2, taking $2a$ as the smallest diameter, the numerical prefactor varies from the value 1.45 stated above to 1.06. From (5) one derives for these samples $2a \simeq 2.0$ nm. This is at variance with the size used by Rousset *et al* (1990) who set $2a = 4.0$ nm, although one of these authors more recently assumed for similar samples a much smaller value (Phalippou *et al* 1991). The size used by Rousset *et al* is based on their TEM observations. On the same samples, Bourret (1988) reports $2a \sim 3.0$ nm, and that value must be considered an upper limit owing to charging effects. The SANS determination is more reliable as it is a real mean, also free of such artefacts.

We now consider the estimate of the lowest Raman vibrational frequency of the particles. For spherical particles of transverse sound velocity v_t, the smallest vibrational frequency is (Lamb 1882)

$$\omega_{\min}/2\pi \simeq 0.8 v_t/2a. \tag{6}$$

In aerogels, the particles are not quite as dense as silica, their density being only $\simeq 1.8$ as opposed to 2.2 g cm^{-3} (Woignier and Phalippou 1987). One knows that the lack of connectivity that this indicates can produce a strong reduction of the sound velocity (Vacher *et al* 1974). To obtain an estimate in the present case, one may assume that the scaling of velocity with density follows the same law as for the aerogels themselves, $(v_t)_{\rho=1.8} \simeq (v_t)_{\rho=2.2} \times (1.8/2.2)^{1.55}$. This was derived from measurements taken under applied pressure (Xhonneux *et al* 1990). A similar relation is found from measurements of Young's modulus on various silica gels (Gronauer *et al* 1986). With the transverse velocity of silica equal to 3700 m s^{-1}, one obtains $v_t \simeq 2700$ m s^{-1}. Using (3) with $2a = 2$ nm, one finds $\omega_{\min}/2\pi \simeq 36$ cm^{-1}. This is close to, but slightly larger than, the position of the lowest frequency particle feature in the measured Raman susceptibility, which is $\simeq 30$ cm^{-1} (Tsujimi *et al* 1988). This is perfectly satisfactory, since any departure from sphericity reduces $\omega_{\min}$.

4.2. *Correlation lengths, and the phonon and fracton spectra*

SANS also determines a quasi Ornstein–Zernike correlation length ξ_ρ. To interpret that value, one should recall how aerogels are formed. During the reaction in the wet state, and before gel formation, clusters grow in the sol. These clusters eventually aggregate at the gel point. The so-called 'grains' seen in gold-coated SEM pictures (figure 1) are likely to be the remainders of these clusters, the fragile matter in between having been destroyed by capillary forces. Hence, the ξ_ρ should somehow be related to the average diameter of those clusters, $2r_0$. Using conventional form factors (e.g. Teixeira 1986) one finds $2r_0 = 2\sqrt{5}\,\xi_\rho$ for isolated near-spherical objects. This relation is expected to hold approximately here, since it is between the clusters that the local density is at its lowest. The values $2r_0$ thus derived from ξ_ρ are observed to be upper bounds of the average cluster size $2r$, reported by Rousset *et al* (1990) and based on their SEM images of gold-coated samples (see table 1). Presumably, the fragile outer part of the clusters tends to be destroyed by the gold, an effect which is of course more important for the lightest clusters ($\rho = 0.11$ g cm^{-3}). Also seen in table 1 is that the value $2r_0$ is remarkably close to that of ξ_{ac} derived from the phonon–fracton crossover observed in Brillouin scattering. The size of the largest fractons, which correspond to the low-frequency end of the fracton regime, must be the cluster size $2r_0$. On the other hand, derivation of the shape of the Brillouin spectra (Courtens *et al* 1988), included the use of a Ioffe–Regel criterion on the phonons (Ioffe and Regel 1960). The good agreement between ξ_{ac} and $2r_0$ now gives

strong support to the hypothesis of a simple phonon–fracton crossover made in the interpretation of the Brillouin spectra.

The fracton dispersion curve, $\omega \propto r^{-D/\tilde{d}}$, can be used to calculate the approximate ratio of the highest to the lowest fracton frequencies, $(r_0/a)^{D/\tilde{d}}$. The lowest fracton frequency occurs at the scale $2r_0$ in agreement with the simple phonon–fracton crossover. The highest fracton frequency should not be confused with the particle mode ω_{min} which does not scale. For the latter reason the estimate of $\tilde{d}$ proposed by Rousset *et al* (1990) is not valid. In fact, as recently shown (Vacher *et al* 1990a), the situation is even more complicated in view of a crossover from bend-dominated to stretch-dominated elasticity that occurs in the fracton regime and produces two distinct values of $\tilde{d}$. From our measurements, one calculates a frequency range which covers the full range over which fractons have been observed, from the phonon–fracton crossover of Brillouin measurements (Courtens *et al* 1988) to the high-frequency end of the Raman measurements (Tsujimi *et al* 1988).

4.3. Scaling of the density and pore-size distribution

We now turn to numerical estimates of the density. It should be clear that one must be very careful not to over-interpret the meaning of prefactors in scaling laws. Usually, orders of magnitude agreements are considered satisfactory. However, we venture in such estimates here since they have been discussed extensively by Rousset *et al* (1990). The scaling of the density is given by

$$\rho(r) = \rho(a)\,(r/a)^{D-3}. \tag{7}$$

The density of the particles is $\rho(a) \simeq 1.8$ (Woignier and Phalippou 1987). Using (7), one calculates the values $\rho(r_0)$ for spherical clusters shown in table 1. These are somewhat larger than the corresponding ρ, and rightly so. Indeed, the clusters pack in some way, leaving around them either voids or material of lower density. It is thus very satisfactory to find that the ratio $\rho/\rho(r_0) \simeq 0.75$. This happens to be approximately the filling ratio of the cubic close-packed structure, and since the clusters are not expected to be exactly close-packed, but rather to form some sort of Bernal packing, this suggests that material of lower density rather than voids must be present between them.

Comments on the interpretation of thermoporometry results are here in order. Thermoporometry is essentially a measurement of the heat of fusion of a liquid that impregnates the porous medium. The principle of the method is that the point of fusion of a liquid in a pore depends on the pore size. As comparative tests such measurements have a definite value. For more quantitative results the method is usually 'calibrated' against a material of 'known' pore-size distribution, such as Vycor glass. In this respect one must note that the shift of the point of fusion is controlled by surface effects (see, e.g. Warnock *et al* 1986). Hence, a detailed quantitative interpretation of a thermoporometry curve for a fractal material (aerogel) based on the calibration against a non-fractal reference of very different pore surface-to-volume ratio (e.g. Vycor) is not warranted. However, the integrated signal which depends only on the total pore volume, and thus on the integral of the heat of fusion, can be quite reliable. Using the scaling relation (7), one can calculate the cumulated specific pore volume per unit mass, V, as a function of the linear pore size, r. This is given by

$$V = [\rho(a) - \rho(r)]/\rho(a)\rho(r) = [(r/a)^{3-D} - 1]/\rho(a). \tag{8}$$

That relation ignores the round-off of the crossover, as seen for example in the simulations in figures 5–7. In this form, the equation applies up to $r = r_0$, beyond which the

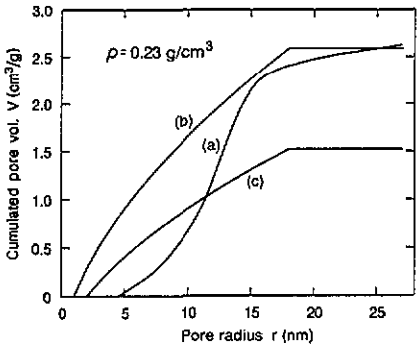

Figure 8. The thermoporometry evaluation of the cumulated pore-size distribution (a), after Rousset *et al* (1990). The scaling prediction from (8), with $2a = 2$ nm (b); and $2a = 4$ nm (c). Note the significant difference between the general shape of (a) and that of (b) and (c). Whereas (b) gives approximately the correct total volume at large r, (c) is obviously much too small.

cumulated volume per unit mass is constant. We now compare the prediction of (8) with the thermoporometry measurement presented by Rousset *et al* for the $\rho = 0.23$ sample. We use two values for $2a$ in (8), namely 2 and 4 nm. The result of the calculation is shown in figure 8. The value $2a = 4$ nm is clearly too large, since it does not allow for a sufficient cumulated pore volume when $r = r_0$ is reached. On the other hand, the value $2a = 2$ nm gives approximately the correct total volume and it is thus much more reasonable. One also observes that the thermoporometry curve does not follow the scaling law. It is clear that equation (1) of Rousset *et al* (1990) is not compatible with their thermoporometry. The reason should presumably be associated with the basic problem of interpretation of thermoporometry data. It is thus erroneous on many counts to conclude from thermoporometry that $2a$ should be 4 nm.

4.4. Opalescence of aerogels

It has been suggested repeatedly (Rousset *et al* 1990, Serughetti 1988, 1990) that the milky appearance of the aerogels may indicate substantial macroporosity at scales as large as the optical wavelength. In this respect, it is useful to recall the observations made on opalescent liquids, in which turbidity is already seen at correlation lengths considerably smaller than the optical wavelength. There are of course no 'macropores' in such liquids. To illustrate this point, we consider the case of a single component fluid, the nematic liquid crystal MBBA just above the liquid-to-nematic phase transition. One degree above the extrapolated critical temperature, T_c, MBBA is rather turbid. However, the value of ξ is only $\simeq 10$ nm (Stinson and Litster 1973, Courtens and Koren 1975), while the optical scattering length is $\simeq 0.9$ cm for the red HeNe laser wavelength (Stinson *et al* 1972). This length is inversely proportional to ξ_ρ^2, to the optical frequency to the fourth power, and to $\Delta\varepsilon^2$, where $\Delta\varepsilon$ is the difference in dielectric constants between the two phases responsible for the turbidity. In the case of MBBA, $\Delta\varepsilon \simeq 1.1$, whereas for aerogels, $\Delta\varepsilon \simeq 2.1$. From the experimental scattering length of MBBA together with the above relations, one calculates, for the densest aerogel used here, an optical scattering length of about 0.7 cm at the green wavelength of the argon-ion laser. A quantitative measurement of this would require some effort in view of the multiple scattering that occurs, especially in the near forward direction. A rough estimate on a slice 0.5 cm thick gave a scattering length of ~ 0.5 cm, which happens to correspond rather well with the above calculation. For the lightest aerogel in table 1, the calculated length becomes 0.02 cm, indicating very high opalescence, as is indeed observed. The point of the above comparison is that the scattering power of the aerogels can be correctly estimated on

the basis of the experimentally measured scattering in a system certainly devoid of macropores. Thus, the observed opalescence of aerogels is fully in line with their description as high-quality fractal materials and cannot be taken as evidence for an anomalously large density of 'macropores'.

5. Conclusions

As amply demonstrated above, our previously published estimates of the various quantities entering the scaling laws are safe ones. The estimates of Rousset *et al* (1990), by contrast, appear biased. The presence of a few macropores is to be expected from the simulations, and the SEM images in figures 2–4 do not suggest that they are in excess of what should be the case for a real fractal. There is no evidence for the large-scale inter-aggregate porosity that Rousset *et al* postulate. There is also no evidence that scaling in ρ fails. For it to hold, it is sufficient that $\rho \propto \rho(\xi)$. The presence of a large excess of macropores could easily invalidate such a simple proportionality. This however does not happen in our mutually self-similar series of samples (Vacher *et al* 1988). Indeed, the scaling of the SANS intensities, a macroscopic and extensive property, proceeds with the same value of D as that of the measured ξ, a microscopic property. A further confirmation is, of course, that the same value of $\tilde{d}$ is found from the scaling of the Brillouin data on many samples, and from the frequency dependence of the density of low-frequency fracton states in one sample (Courtens *et al* 1990, Vacher *et al* 1990a).

The main positive element of our analysis is that the ratio ξ_{ac}/ξ_ρ is now clearly understood as being the ratio between the diameter of the fractal clusters and their Ornstein–Zernike correlation length. This observation implies that ξ_{ac} is essentially the size of the largest fracton. On the other hand, ξ_{ac} was derived from our Brillouin data essentially as the length at which the Ioffe–Regel criterion applies, i.e. where the phonon scattering length becomes equal to its wavelength. This means that the phonon–fracton crossover and the Ioffe–Regel limit coincide fairly well, supporting the line shapes that were used to analyse the Brillouin spectra, as well as the scaling of the data, for this sample series. This gives additional strong support to our Brillouin scattering determination of D and $\tilde{d}$. Another confirmation of this is that the crossover frequency determined in Brillouin scattering is equal to the phonon–fracton one directly measured on the density of states by inelastic neutron scattering (Courtens *et al* 1990). Below the crossover, located typically at ~1 GHz, Brillouin scattering demonstrates the existence of well-behaved phonons, and this also cannot be reconciled with a large-scale inter-aggregate porosity.

In the Raman susceptibility, the peak at ~1000 GHz is to be assigned to particles. The structural–fractal vibrations occur below that frequency. Above it, the excitations are confined to the constitutive particles, and their frequencies bear no relation to the fractal structure associated with the aerogel porosity. The scaling in ω of the Raman intensity has not been discussed here. The main reason is that this scaling involves at least one additional index, as explained in detail by Alexander (1989), and this goes beyond the object of the present work. Also, the subject remains to this day a matter of considerable discussion (see, e.g. Montagna *et al* 1990). We expect to present the scaling of the Raman intensities in a future publication (Alexander *et al* 1991).

Acknowledgments

Two of us (RV and EC) thank Professor J Pelous for his valuable comments, and for communicating the preprint of Rousset *et al* in September 1990. We also thank Dr B Michel and Dr W Denk for the suggestion to use, and for the help with, the Pt/C coating. Comments on the manuscript by Dr M Kolb are gratefully acknowledged.

References

Alexander S 1989 *Phys. Rev.* B **40** 7953
Alexander S, Courtens E, Stoll E and Vacher R 1991 in preparation
Alexander S and Orbach R 1982 *J. Physique Lett.* **43** L625
Bourret A 1988 *Europhys. Lett.* **6** 731
Courtens E and Koren J 1975 *Phys. Rev. Lett.* **35** 1711
Courtens E, Lartigue C, Mezei F, Vacher R, Coddens G, Foret M, Pelous J and Woignier T 1990 *Z. Phys.* B **79** 1
Courtens E, Pelous J, Phalippou J, Vacher R and Woignier T 1987 *Phys. Rev. Lett.* **58** 128
Courtens E and Vacher R 1989 *Proc. R. Soc.* A **423** 55
Courtens E, Vacher R, Pelous J and Woignier T 1988 *Europhys. Lett.* **6** 245
Fleischmann M, Tildesley D J and Ball R C (ed) 1989 Fractals in the natural sciences *Proc. R. Soc.* A **423**
Fricke J (ed) 1986 *Aerogels* (Berlin: Springer)
Gronauer M, Kadur A and Fricke J 1986 *Aerogels* ed J Fricke (Berlin: Springer) p 167
Ioffe A F and Regel A R 1960 *Prog. Semicond.* **4** 237
Kapitulnik A, Aharony A, Deutscher G and Stauffer D 1983 *J. Phys. A: Math. Gen.* **16** L269
Lamb H 1882 *Proc. Math. Soc. London* **13** 187
LeMay J D, Hopper R W, Hrubesh L W and Pekala R W 1990 *MRS Bulletin* **XV** 41
Montagna M, Pilla O, Viliani G, Mazzacurati V, Ruocco G and Signorelli G 1990 *Phys. Rev. Lett.* **65** 1136
Phalippou J, Ayral A, Woignier T, Quinson J F, Pauthe M and Chatelut M 1991 *Europhys. Lett.* **14** 249
Porod G 1951 *Kolloid Z.* B **124** 83
Richter D, Dianoux A J, Petry W and Teixeira J (ed) 1989 *Dynamics of Disordered Materials* (Berlin: Springer)
Rousset J L, Boukenter A, Champagnon B, Dumas J, Duval E, Quinson J F and Serughetti J 1990 *J. Phys.: Condens. Matter* **2** 8445
Schmidt P W 1991 *J. Appl. Crystallogr.* at press
Serughetti J 1988 1990 (private communications)
Stauffer 1986 *On Growth and Form* (ed) H E Stanley and N Ostrowsky (Dordrecht: Nijhoff) pp 79–100
Stinson T W and Litster J D 1973 *Phys. Rev. Lett.* **30** 688
Stinson T W, Litster J D and Clark N A 1972 *J. Physique Suppl.* **33** C1 69
Teixeira J 1986 *On Growth and Form* (ed) H E Stanley and N Ostrowsky (Dordrecht: Nijhoff) pp 145–62
Tsujimi Y, Courtens E, Pelous J and Vacher R 1988 *Phys. Rev. Lett.* **60** 2757
Vacher R, Courtens E, Coddens G, Heidemann A, Tsujimi Y, Pelous J and Foret M 1990a *Phys. Rev. Lett.* **65** 1008
Vacher R, Courtens E and Pelous J 1990b *La Recherche* **21** 426
Vacher R, Delsanti M, Pelous J, Cecchi L, Winter A and Zarzycki J 1974 *J. Mater. Sci.* **9** 829
Vacher R, Phalippou J, Pelous J and Woignier T (ed) 1989 *J. Physique Suppl.* C4
Vacher R, Woignier T, Pelous J and Courtens E 1988 *Phys. Rev.* B **27** 6500
Warnock J, Awschalom D D and Shafer M W 1986 *Phys. Rev. Lett.* **57** 1753
Woignier T and Phalippou J 1987 *J. Non-Cryst. Solids* **93** 17
Xhonneux P, Courtens E, Pelous J and Vacher R 1990 *Europhys. Lett.* **10** 733